POLYMODE NEWS

No. 63 March 23, 1979

In this issue:

Lutjeharms, Baker: Geographic variations in intensities and scales of motion in the Southern Ocean
Seidov, Zhicharev: On the numerical scheme used in the Eulerian-Lagrangian model of the ocean circulation
POLYMODE OFFICE NOTES: POLYMODE Preliminary Scientific Results volumes available; NODC 24-hour Ocean Data Message Center established

GEOGRAPHIC VARIATIONS IN INTENSITIES AND SCALES OF MOTION IN THE SOUTHERN OCEAN

by Johann Lutjeharms and Jim Baker

In a recent contribution (POLYMODE News No. 52), we described an analysis of the historic hydrographic data of the Southern Ocean which attempted to resolve mesoscale features in the general region of the Antarctic Circumpolar Current (ACC). We found that in this area mesoscale disturbances with scales (interpreted as diameters) of between 100 km to 300 km may be found in about 20% of all hydrographic and bathythermographic station lines. A preliminary statistical analysis showed the existence of a geographic pattern in the occurrence and intensity of mesoscale disturbances. We have now refined and adjusted the geographic grids used for the statistical analysis; this note reports the results of these more recent analyses.

Any statistical analysis of historic hydrographic data in the Southern Ocean is immediately hamstrung by the geographically inhomogeneous distribution of stations and by the strong bias towards stations undertaken during the austral summer (POLYMODE News No. 52). A further restriction involves the limited number of stations that exceed 1000 m in depth. We have therefore confined our investigation of the dynamics to the upper 1000 m since simultaneous calculations, to be reported elsewhere, indicate that this is representative of the total water column.

As a variable for the analysis, the dynamic interval 0/1000 dbar was thus employed and this was detrended using the mean dynamic topography produced by Gordon, Molinelli, and Baker (1978). The standard deviation of this variable for each 10°x10° area is shown in Figure 1. The effect of limited data is obvious (note the number of areas possessing fewer than ten stations). Nevertheless, a distinct pattern is evident. Values close to the Antarctic continent tend to be smaller than those further to the north. In addition, a number of areas are conspicuous for high variability. These include the terminal area of the Agulhas Current which lies to the south of Africa (value 256), the Kerguelen Plateau (71-115), the New Zealand Plateau/Macquarie Ridge (72-127), the Pacific Mid-Ocean Ridge (88-106), and the Drake Passage/Scotia Sea/Falkland Plateau (100-148). These areas have one of two factors in common: either they represent a prominent bottom topography feature which is crossed by the ACC, or they are located in the terminal region of a major current.

In order to resolve spatial scales, calculations of the estimated spatial structure functions (ESF) have been made (Dantzler, 1976):

$$E[B_f(\underset{\sim}{r})] = \frac{1}{n} \sum^{n} \{f(\underset{\sim}{\ell}) - f(\underset{\sim}{\ell} + \underset{\sim}{r})\}^2$$

where $B_f(\underset{\sim}{r})$ represents the structure function, n the number of station pairs for that spatial interval, r the spatial interval, and f the dynamic variable employed. We used spatial intervals of 100 km from 0-1500 km. Since the calculations for the ESF are subjected to a time/distance filter (Lutjeharms, 1977b), fewer station pairs are available. To fulfill the requirements for statistical significance while retaining the maximal spatial resolution, a different network was designed, so that the number of available station pairs in each block is essentially the same (Figure 2).

(continued page 4)

POLYMODE OFFICE NOTES

Volumes I and II of the POLYMODE Preliminary Scientific Results, covering the experimental, theoretical, and numerical modelling programs, have been mailed to all POLYMODE scientists. Additional copies of both volumes are available from the POLYMODE Executive Office, Room 54-1418, Massachusetts Institution of Technology, Cambridge, MA 02139.

- - - - - - - - - - - - - -

The National Oceanographic Data Center has recently established a 24-hour Ocean Data Message Center to provide ocean data users better access to the NODC for making service requests. The center is on a pilot project basis; if successful, it will be incorporated into the NODC's suite of regular services. Requests received at the message center will be handled during normal working hours by NODC's marine information specialists. The 24-hour telephone number is: (202) 634-7502.

The POLYMODE* News is produced at the Woods Hole Oceanographic Institution. It is edited by Ferris Webster and Catherine Herrity.

Material of interest for this newsletter may be sent to Catherine Herrity at the Woods Hole Oceanographic Institution, Woods Hole, MA, 02543, Telephone (617) 548-1400, ext. 2550, TWX 710-346-6601; or to Ferris Webster at NOAA/RD, 6010 Executive Blvd, Rockville, MD, 20852, Telephone (301) 443-8344.

*POLYMODE is derived from the names of the USSR POLYGON experiments and the Mid-Ocean Dynamics Experiment (MODE).

CONTRIBUTORS

Dr. James Baker Jr.
Pacific Marine Environmental Laboratory/NOAA
3711 15th Avenue NE
Seattle WA 98105
(206) 543-7160

Dr. Johann R. E. Lutjeharms
National Research Institute for Oceanology
P. O. Box 320
Stellenbosch 7600 SOUTH AFRICA
71010

Dr. D. G. Seidov
P. P. Shirshov Institute of Oceanology
Academy of Sciences USSR
ul. Krasikova, 23
USSR Moscow 117218

Dr. G. M. Zhicharev
P. P. Shirshov Institute of Oceanology
Academy of Sciences USSR
ul. Krasikova, 23
USSR Moscow 117218

ERRATUM

(POLYMODE News No. 62)

The present address for contributor Dr. Peter Müller is: Pierce Hall, Harvard University, Cambridge MA 02138.

ACKNOWLEDGEMENT

The POLYMODE News is produced with support from the International Decade of Ocean Exploration (IDOE) of the National Science Foundation, the Office of Naval Research, and the National Oceanic and Atmospheric Administration.

1/750

ON THE NUMERICAL SCHEME USED IN THE EULERIAN-LAGRANGIAN MODEL OF THE OCEAN CIRCULATION

by D. G. Seidov and G. M. Zhicharev

An Eulerian-Lagrangian model of ocean currents (Seidov, 1978) was recently used to simulate synoptic-scale motions in a baroclinic ocean (Seidov, 1978; Seidov and Rusetski, POLYMODE News No. 46). The advective part of this model was based on the Lax-Wendroff scheme, also used by Leith (1965) and Crowley (1968). Crowley compared this scheme with one that was second-order in time, as we shall do for the particular case of the large-scale wind-driven circulation in a barotropic ocean on a β-plane. The experiment will show the capability of this scheme to represent advective processes in comparison with more precise modelling.

The scheme for the two-dimensional case may be reviewed by considering a quantity that is advected by currents. The equation $\frac{\partial \psi}{\partial t} = 0$ may be represented by a Taylor expansion

$$\psi^{n+1}=\psi^n+\alpha\frac{\partial\psi^n}{\partial x}+\alpha^2\frac{\partial^2\psi^n}{\partial x^2}+\delta\frac{\partial\psi^n}{\partial y}+\delta^2\frac{\partial^2\psi^n}{\partial y^2}+\frac{1}{2}\alpha\delta\frac{\partial^2\psi^n}{\partial x\partial y}\ , \quad (1)$$

where $\alpha = -u^n\Delta t$; $\delta = -v^n\Delta t$; u,v directed to the east and north respectively; n is the number of time steps; Δt is the time step, $\Delta t = t^{n+1}-t^n$.

This scheme has a first order of approximation in time, and second in space. Artificial viscosity does not seem to be essential (Seidov, 1978), nor does it play a significant role in the experiments.

Two numerical experiments were performed. The first one was carried out with the help of a traditionally arranged Arakawa scheme for the Jacobian in the vorticity balance equation. The second one was done with a splitting procedure and equation (1), as used for advection modelling.

For the circulation in a flat-bottomed, barotropic rectangular basin on a β-plane, the vorticity balance may be represented (Bryan, 1963; Veronis, 1966):

$$\frac{\partial \eta}{\partial t} + RJ(\psi,\eta) + \frac{\partial \psi}{\partial x} - \varepsilon\nabla^2\eta = \mathrm{rot}\vec{\tau}, \quad (2)$$

where $R = W/H\beta^2L^3$; $\varepsilon = AL/\beta L^3$; ψ is total streamfunction; η is vorticity; W,L are characteristic values of wind stress and the dimension of the basin; $\beta = 0.2\ 10^{-12}$; AL is the coefficient of horizontal turbulent friction; and J is the Jacobian. The boundary condition for (2) is $\eta|_\Sigma = 0$ (free slip). The total flux is obtained from

$$\nabla^2\psi = \eta \qquad \text{with } \psi|_\Sigma = 0, \quad (3)$$

where Σ is the lateral boundary.

In the first experiment, (2) and (3) were solved as was done by Bryan (1963) and Veronis (1966), with the iterative method for (3). In the second experiment, equation (2) was split as follows:

$$\frac{\partial \eta}{\partial t} + \frac{\partial \psi}{\partial x} - \varepsilon\nabla^2\eta = \mathrm{rot}\vec{\tau}, \quad (4a)$$

$$\frac{\partial \eta}{\partial t} + u\frac{\partial \eta}{\partial x} + v\frac{\partial \eta}{\partial y} = 0 \quad (4b)$$

where $u = -\frac{1}{H}\frac{\partial \psi}{\partial y}$, $v = \frac{1}{H}\frac{\partial \psi}{\partial x}$.

Two calculations were performed in each experiment. The first one deals with the slight non-linearity (SN) of the motions with $R^{1/2} = 0.03$ and $\varepsilon^{1/3} = 0.03$. The second calculation represents a stronger non-linear case (N) in which $R^{1/2} = 0.05$ and $\varepsilon^{1/3} = 0.03$.

Figure 6 shows the kinetic energy in the SN case for both experiments. At the moment when the circulation becomes stable, the difference between the energy curves for the two schemes is about 8%. Figures 7 and 8 show the normalized ψ functions for the SN and N cases. There is rather good qualitative and quantitative agreement.

We conclude that first-order time schemes can be applied to numerical ocean circulation models. We prefer the Lax-Wendroff scheme in this manner because of its effectiveness (especially for the modelling of three-dimensional advection). There are only two fields -- previous (n), and current (n+1) -- in the core of the computer (instead of three for the second-order schemes), with no significant loss of accuracy.

References

Bryan, K. (1963) A numerical investigation of a non-linear model of a wind driven ocean. J. Atmos. Sci., *20(6)*, 594-606.

Crowley, W. P. (1968) Numerical advection experiment. Mon. Weather Rev., *96(1)*, 1-11.

Leith, C. E. (1965) Numerical simulation of the Earth's atmosphere. Methods Comput. Phys., *5*.

Sarkisyan, A. S., D. G. Seidov, and E. V. Semyonov (1978) A numerical model of a synoptic ocean currents. Oceanology, *16(1)*, 5-10.

Seidov, D. G. (1977) Numerical model of circulation of the baroclinic ocean. Izv. USSR Acad. Sci., Phys. Atmos. Ocean., *13(8)*, 867-875.

Seidov, D. G. (1978) Numerical scheme for synoptical eddies in the ocean. Izv. USSR Acad. Sci., Phys. Atmos. Ocean., *14(7)*, 757-767.

Veronis, G. (1966) Wind driven ocean circulation. Part 2. Deep-Sea Res., *13*, 31-50.

Although the resolution has been reduced considerably, the general pattern present in Figure 1 is once more apparent in Figure 2 which gives the values for the ESF of the 0/1000 dbar dynamic interval for the spatial interval 100-200 km. This interval was chosen because we believe it to be typical of the dimensions of what appear to be the majority of mesoscale disturbances in the Southern Ocean (Lutjeharms and Baker, POLYMODE News No. 52), but the basic pattern discernible here remains essentially unchanged for a wide range of spatial intervals.

The reason for this behavior is immediately apparent from an inspection of three representative ESFs portrayed in Figure 3 for the areas referenced as such in Figure 2. All rise to a near-maximum value at about 150 km with little substantial increase for greater separations. With few exceptions, this is the general form for all ESFs calculated for the various parts of the Southern Ocean. Since the ESF is a cumulative function, the implication is that the total contribution to the variance occurs at distances of less than 150 km. Since the station spacing is approximately 100 km, it is not possible to say from these data whether significant energy lies at smaller scales. This result is consistent with the coherence scales of less than 80 km found by Bryden and Pillsbury (1977) from year-long current meter moorings in the Drake Passage and also with the estimated Rossby radius of deformation for the area of 10-60 km.

Removing an alternative mean, independently calculated, has shown that this result is not dependent on the manner in which the data were detrended. A notable exception to this general form of the ESF is the one for the terminal region of the Agulhas Current (Lutjeharms, 1977b) which shows a significant peak at about 200 km. This is slightly larger than the dimensions found for mesoscale phenomena in the area just to the north (Lutjeharms, 1977a).

One mechanism proposed for the formation of eddies and other mesoscale disturbances in the Southern Ocean is instability in the zonal flow of the ACC. The pinching off of an eddy has already been observed by Joyce and Patterson (1977) in the Drake Passage. In order to test such an hypothesis for the ocean as a whole, a grid was constructed with areas parallel to the Antarctic Polar Front, which coincides with the core of the ACC. The standard deviation of the detrended dynamic interval for this grid is presented in Figure 4. To include sufficient numbers of stations in each area, the areas had to be made rather long zonally, thus complicating conclusions by including a number of areas previously shown to have differing levels of variability. In the South Atlantic the southernmost areas will, for instance, be contaminated by high variability originating in the terminal areas of the Falkland and Agulhas Currents, as seen in Figure 1. In any case, a definite pattern appears: increasing values of the standard deviation on approaching the Polar Front and decreasing values moving away from it. This holds true particularly south of the Front. One possible conclusion is that the ACC acts as an eddy-generating mechanism along its full length. Another is that the hydrographic data are contaminated by meanders of the ACC, not eddies. In either case, there is significant energy in the space scales less than 150 km.

Three possible generating mechanisms for mesoscale turbulence are thus suggested (Figure 5) for the Southern Ocean: the termination of the Agulhas Current; the interaction of the ACC and major bottom topographic features such as mid-ocean ridges and plateaus; and, lastly, instabilities of the ACC itself. It is interesting to compare these results with those found by Wyrtki, Magaard and Hager (1976). They calculated the eddy kinetic energy of the world oceans making use of observations of ships' drift. Where results for the ACC are available, they show moderately high eddy energy values; the Agulhas Current is also conspicuous for its extremely high energy contribution to the Southern Ocean.

References

Bryden, H. L. and R. D. Pillsbury (1977) Variability of deep flow in the Drake Passage. J. Phys. Oceanogr., 7, 803-810.

Dantzler, H. L. (1976) Geographic variations in intensity of the North Atlantic and North Pacific oceanic eddy fields. Deep-Sea Res., 23(9), 783-794.

Gordon, A. L., E. Molinelli, and T. Baker (1978) Large-scale relative dynamic topography of Southern Ocean. J. Geophys. Res., 83, 3023-3032.

Joyce, T. M. and S. L. Patterson (1977) Cyclonic ring formation at the Polar Front Zone in the Drake Passage. Nature, Lond., 265(5590), 131-133.

Lutjeharms, J. R. E. (1977a) Time variations in the spatial scales and intensities of ocean circulation in the vicinity of the Cape of Good Hope. Tellus, 29, 375-381.

Lutjeharms, J. R. E. (1977b) Meso-scale dynamics in the Southern Ocean: a statistical analysis of historic data. Ph.D. dissertation, University of Washington, 181 pp.

Wyrtki, K., L. Magaard, and J. Hager (1976) Eddy energy in the oceans. J. Geophys. Res., 81(15), 2641-2646.

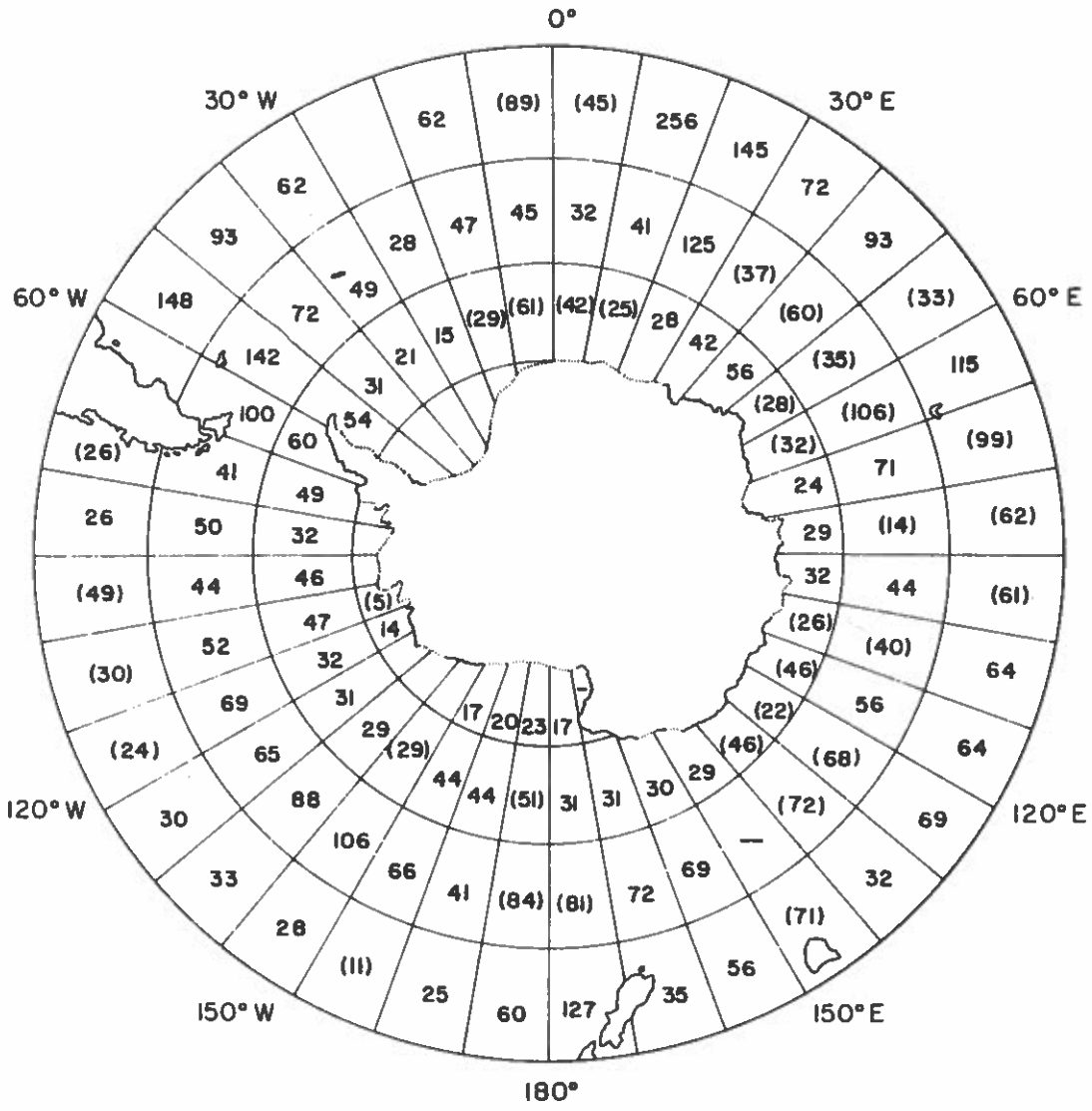

Values for the standard deviation (in units of 10^{-2} m^2/s^2) of the dynamic interval 0/1000 dbar for each Marsden Square of the Southern Ocean. The mean trend removed from the data was that according to Gordon et al. (1978). Figures in parentheses denote values supported by less than ten hydrographic stations. Blank areas denote squares in which there were fewer than two hydrographic stations to 1000 m.

Figure 1 (Lutjeharms and Baker)

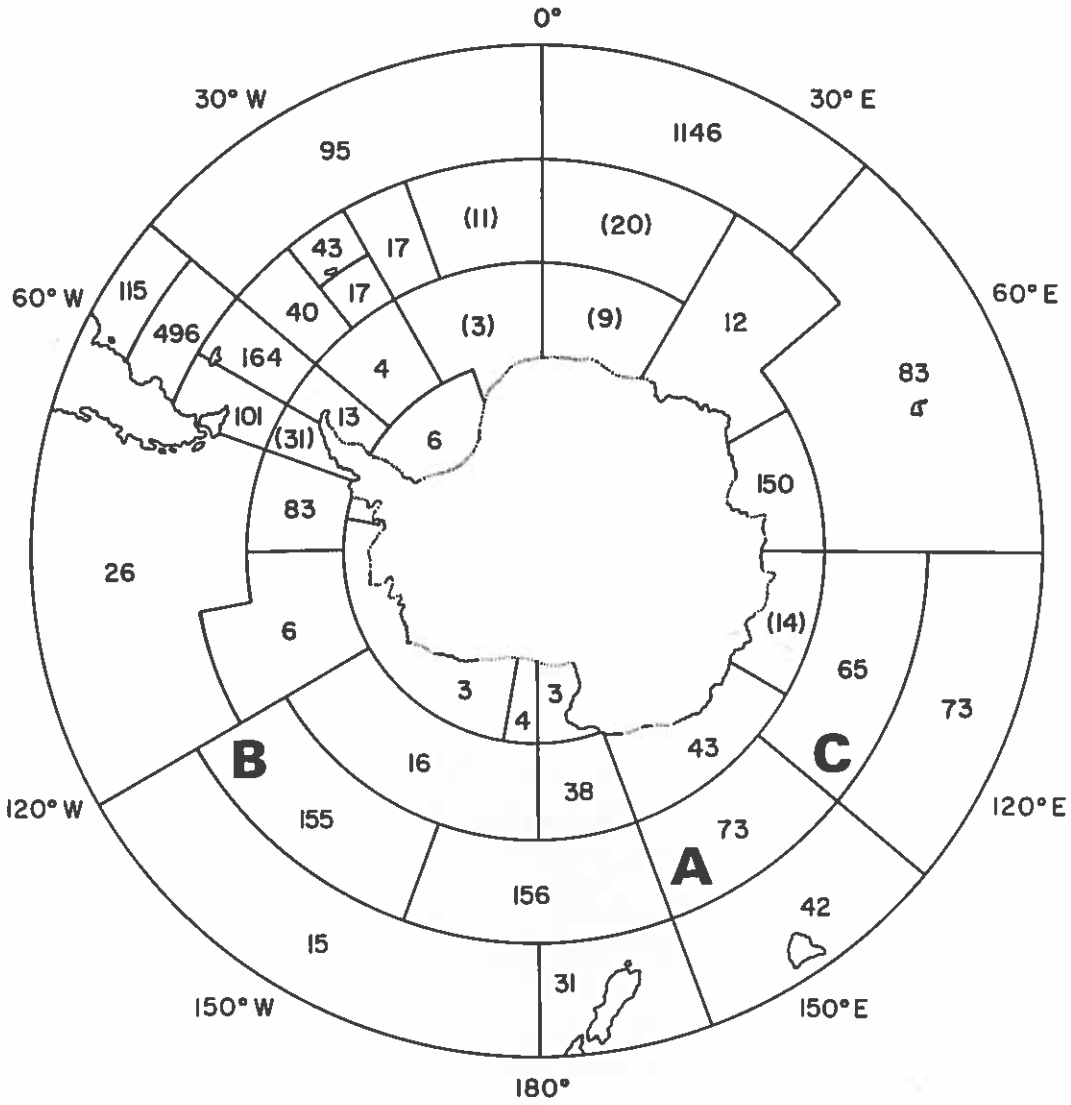

Values of the estimated spatial structure function for geographic areas of different size in the spatial interval 100-200 km using as dynamic variable the detrended dynamic interval 0/1000 dbar. Values are in units of 10^{-2} m^4/s^4 and those in parentheses indicate values calculated using fewer than 10 station pairs. The structure functions for the areas referenced are portrayed in Figure 3.

Figure 2 (Lutjeharms and Baker)

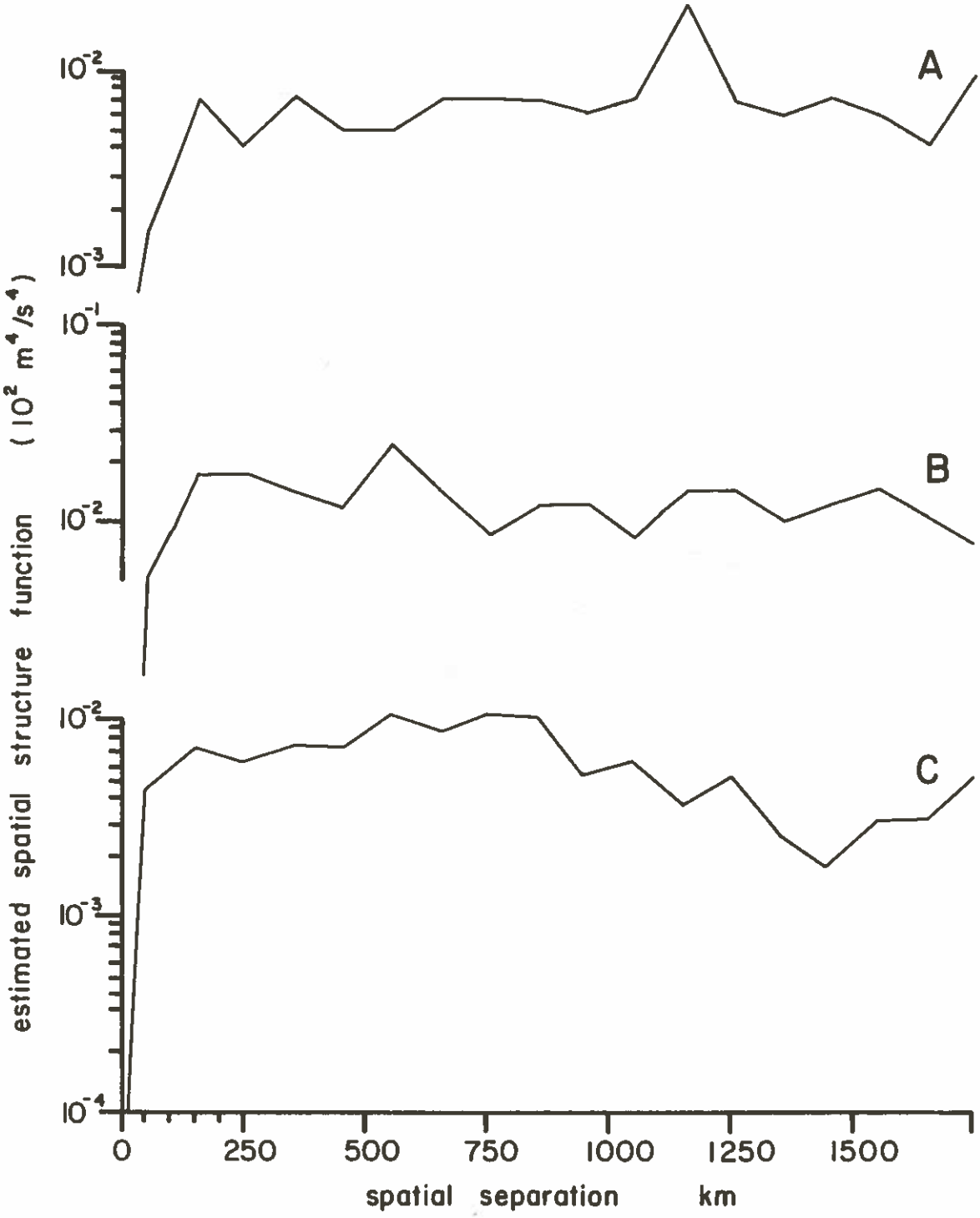

The spatial structure functions for three geographic areas indicated in Figure 2. The dynamic variable used for the calculation was the detrended dynamic interval 0/1000 dbar. The curves have been offset on the ordinate to separate them.

Figure 3 (Lutjeharms and Baker)

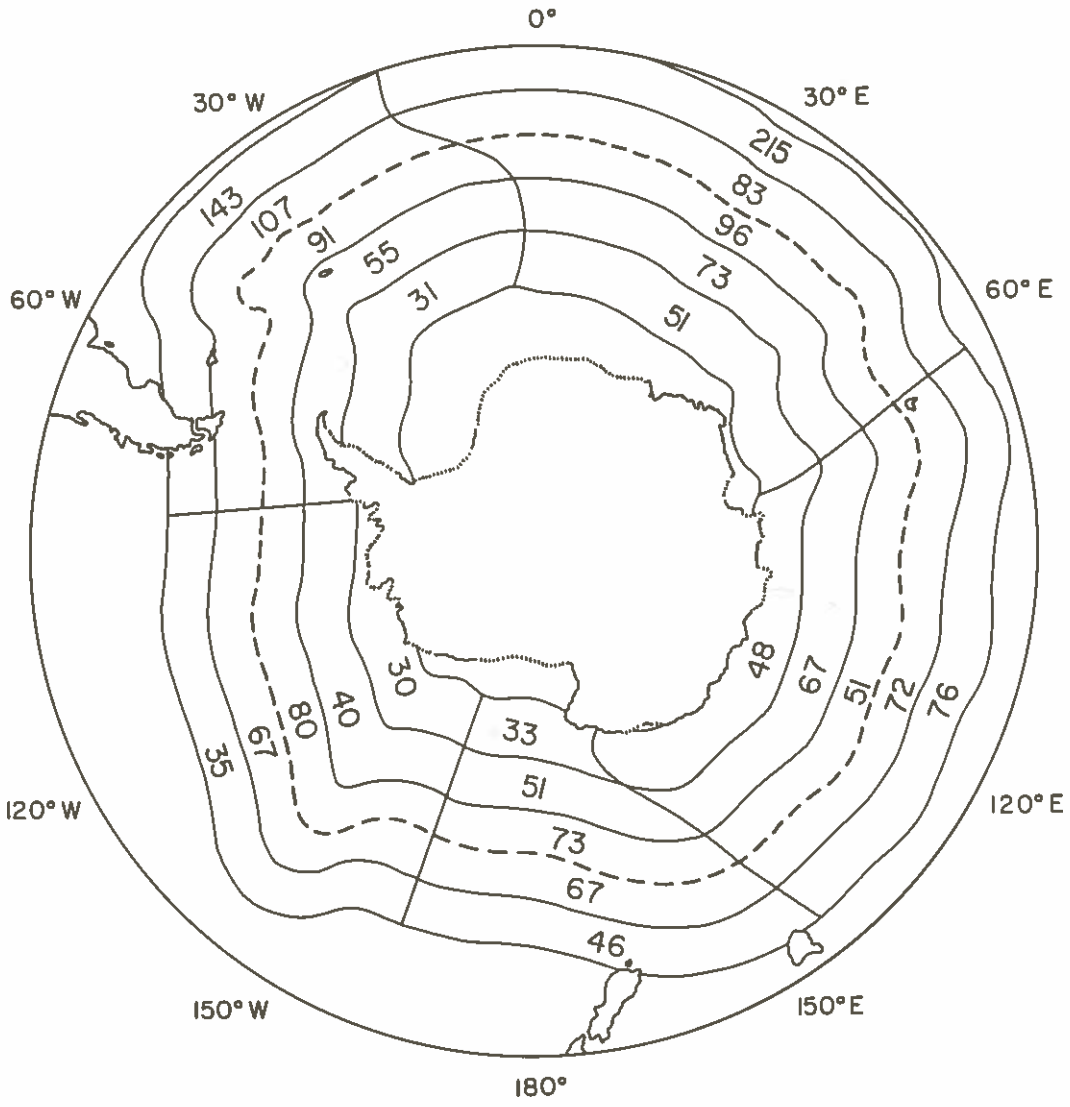

Values of the standard deviation of the detrended dynamic interval 0/1000 dbar for geographic areas parallel to the Antarctic Polar Front. Units are 10^{-2} m^2/s^2. The heavy dashed line indicates the mean position of the Antarctic Polar Front.

Figure 4 (Lutjeharms and Baker)

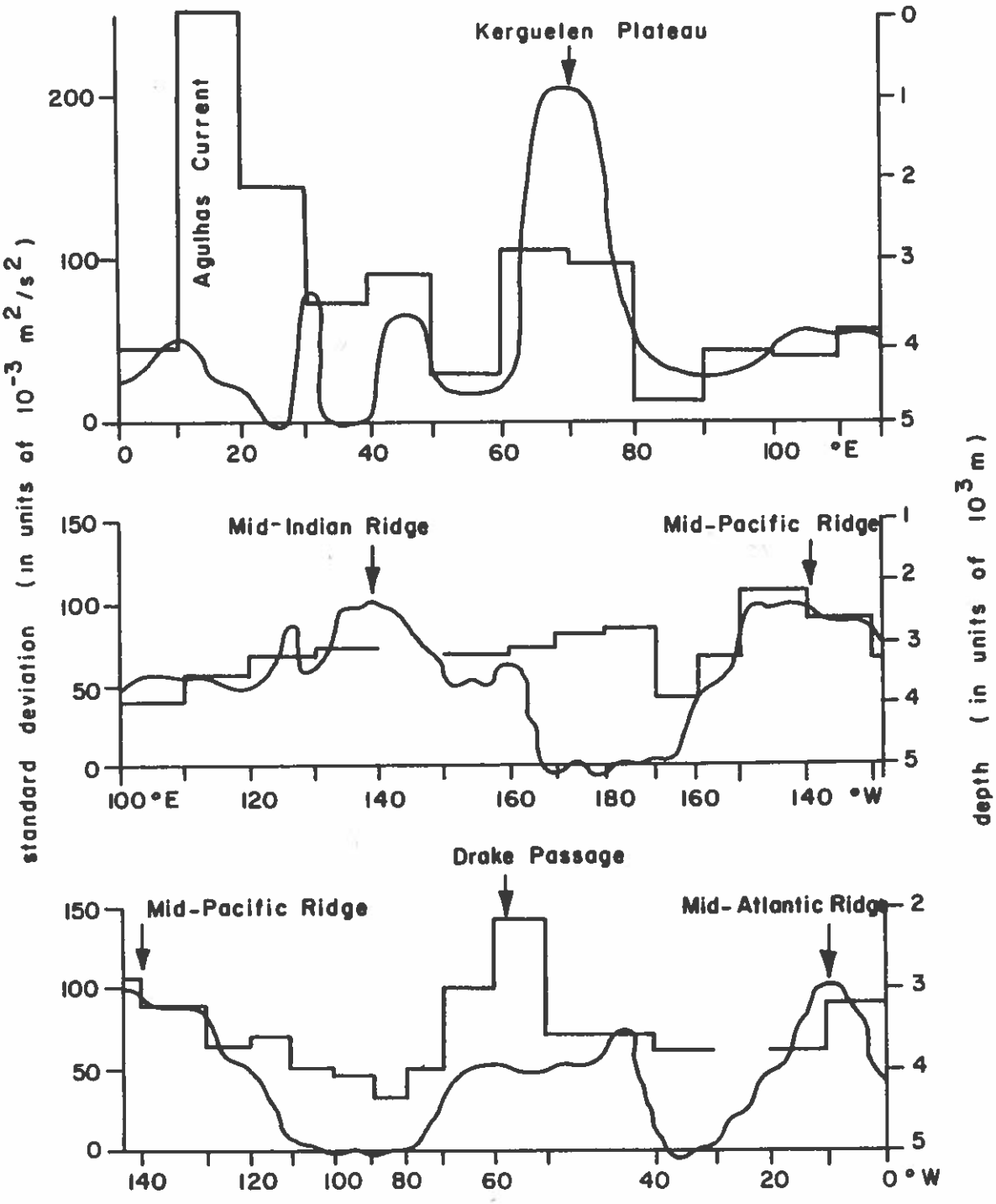

Curve depicting bottom topography along the main axis of the Antarctic Circumpolar Current and a histogram of standard deviation of dynamic interval 0/1000 dbar for each Marsden Square (see Figure 1). The longitudes of some features are labelled.

Figure 5 (Lutjeharms and Baker)

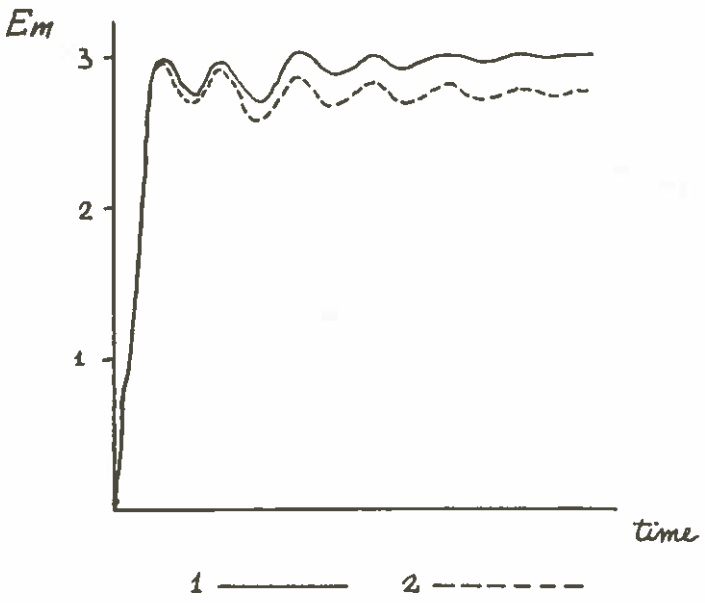

The mean kinetic energy Em (cgs) in the slightly non-linear case for the first experiment (solid line) and the second experiment (dashed line).

Figure 6 (Seidov and Zhicharev)

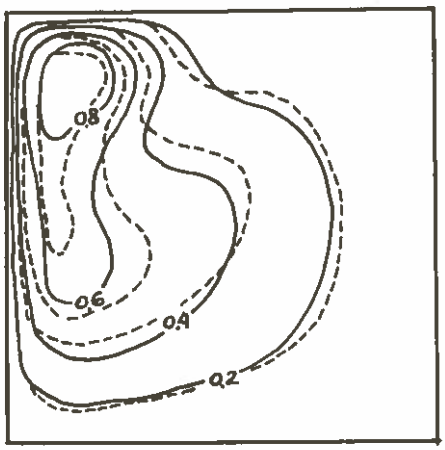

The total streamfunction ψ/ψ_{max} in the slightly non-linear case for the first experiment (solid line), $\psi_{max}=18.4\ 10^{12}cm^3s^{-1}$, and the second experiment (dashed line), $\psi_{max}=16.9\ 10^{12}cm^3s^{-1}$.

Figure 7 (Seidov and Zhicharev)

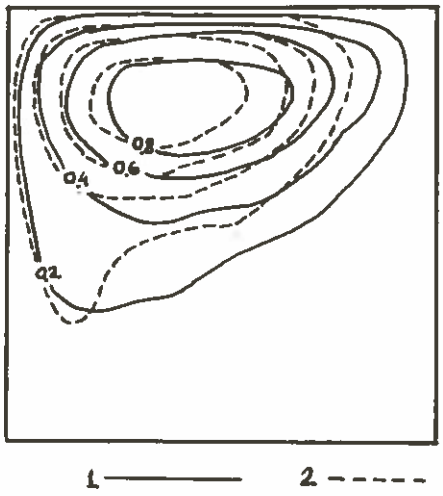

The total streamfunction ψ/ψ_{max} in the stronger non-linear case for the first experiment (solid line), $\psi_{max}=96.9\ 10^{12}cm^3s^{-1}$, and the second experiment (dashed line), $\psi_{max}=82.8\ 10^{12}cm^3s^{-1}$.

Figure 8 (Seidov and Zhicharev)